Smart Molecular Helical Springs as Tunable Receptors

Ok-Sang Jung,*,† Yun Ju Kim,† Young-A Lee,† Jong Ku Park,† and Hee K. Chae‡

Contribution from the Materials Chemistry Laboratory, Korea Institute of Science and Technology, Seoul 136-791, Korea, and Department of Chemistry, Hankuk University of Foreign Studies, Yongin 449-791, Korea

Received May 11, 2000

Abstract: The rational construction and operation of an ideal helical spring has been investigated. The infinite helices, $[Ag(Py_2O)]X$ (Py_2O = 3,3′-oxybispyridine; X^- = NO_3^-, BF_4^-, ClO_4^-, and PF_6^-), have been constructed in high yield via cooperative effects of the skewed conformer of Py_2O and the potential linear geometry of the N−Ag(I)−N bond. Crystallographic characterization reveals that the polymer framework is an ideal cationic cylindrical helix and that its counteranions are pinched in two columns inside the helix. The four anions have been exchanged for each other in an aqueous solution without destruction of the helical skeleton. In particular, $[Ag(Py_2O)]NO_3$ prepared by the counteranion exchange can be isolated as crystals suitable for X-ray crystallography in water. The helical pitch is reversibly stretched via the counteranion exchange from 7.430(2) to 9.621(2) Å, and is exactly proportional to the volume of the anion guests. This pitch-tuning is attributed to subtle change in the nonrigid dihedral angles between two pyridyl groups around O and Ag atoms that act as hinges within the helical subunit. Thermal analyses indicate that the helical compounds are stable up to 231−332 °C in the solid state.

Introduction

Molecular materials with helical morphology have practical implication in multidisciplinary areas such as templating precursors,[1] memory devices,[2,3] biomimetic chemistry,[4,5] chiral chemistry,[6] DNA,[7] and structural biology.[8] Control of such nature-derived motifs has now advanced to the point where the task may be addressed.[9] In particular, *a fundamental feature of a typical cylindrical helix is its elastic ability to return to its usual shape*, i.e., to function as a "spring" within the tunable pitch. Low-dimensional functional topologies by the assembly of metal coordination species can be specifically designed according to the selection of basic components such as the coordination geometry of the metal ions, the binding site of the donating atoms, and the length of the spacer.[10−18] Various ligands have been used for molecular helical building blocks,[19] but exploitation of 3,3′-oxybispyridine (Py_2O) as a helical component has until recently remained unprecedented. The ligand possesses stable skewed conformers with nonrigid interannular dihedral angles between two pyridyl groups.[20,21] The silver(I) ion can be employed as an angular directional unit, as it is known to preferably exhibit a linear or T-shaped coordination mode.[18,22] Nitrate, tetrafluoroborate, perchlorate, and hexafluorophosphate that frequently appear in chemistry, environmental pollution, disease pathway, and biological processes[23,24] were selected as the anionic balancer of the cationic skeleton.

In the present report we describe studies on the rational construction and operation of an ideal cylindrical helix using the concepts of a skewed conformational unit with nonrigid interannular dihedral angles. This helix is an unprecedented tunable spring that is reversibly operated by a counteranion exchange.

Experimental Section

Materials and Physical Measurements. AgX and NaX (X^- = NO_3^-, BF_4^-, ClO_4^-, and PF_6^-) were purchased from Strem Co. and

* Address correspondence to this author. Fax: 82-2-958-5089. E-mail: oksjung@kist.re.kr.

†Korea Institute of Science and Technology.

‡ Hankuk University of Foreign Studies.

(1) Dietrich-Bucheker, C. O.; Guilhem, J.; Pascard, C.; Sauvage, J.-P. *Angew. Chem., Int. Ed. Engl.* **1990**, *29*, 1154−1156.
(2) Yashima, E.; Maeda, K.; Okamoto, Y. *Nature* **1999**, *399*, 449−451.
(3) Piguet, C.; Bernardinelli, G.; Hopfgartner, G. *Chem. Rev.* **1997**, *97*, 2005−2062.
(4) Hannak, R. B.; Färber, G.; Kornat, R.; Kräutler, B. *J. Am. Chem. Soc*. **1997**, *119*, 2313−2314.
(5) Orr, G. W.; Barbour, L. J.; Atwood, J. L. *Science* **1999**, *285*, 1049−1052.
(6) Biradha, K.; Seward, C.; Zaworotko, M. J. *Angew. Chem., Int. Ed. Engl*. **1999**, *38*, 492−494.
(7) Chalmers, R.; Guhathakurta, A.; Benjamin, H.; Kleckner, N. *Cell* **1998**, *93*, 897−908.
(8) Klug, A. *Angew. Chem., Int. Ed. Engl*. **1983**, *22*, 565−582.
(9) Rowan, A. E.; Nolte, R. J. M. *Angew. Chem., Int. Ed.* **1998**, *37*, 63−68.
(10) Venkatarataraman, D.; Gardner, G. B.; Lee, S.; Moore, J. S. *J. Am. Chem. Soc*. **1995**, *117*, 11600−11601.
(11) Yaghi, O. M.; Li, H.; Davis, C.; Richardson, D.; Groy, T. L. *Acc. Chem. Res*. **1998**, *31*, 474−484.
(12) Kitagawa, S.; Kondo, M. *Bull. Chem. Soc. Jpn*. **1998**, *71*, 1739−1753.
(13) Gudbjartson, H.; Biradha, K.; Poirier, K. M.; Zaworotko, M. J. *J. Am. Chem. Soc*. **1999**, *121*, 2599−2600.
(14) Chui, S. S.-Y.; Lo, S. M.-F.; Charmant, J. P. H.; Orpen, A. G.; Williams, I. D. *Science* **1999**, *283*, 1148−1150.
(15) Jung, O.-S.; Pierpont, C. G. *J. Am. Chem. Soc*. **1994**, *116*, 2229−2230.
(16) Jung, O.-S.; Park, S. H.; Kim, D. C.; Kim, K. M. *Inorg. Chem*. **1998**, *37*, 610−611.
(17) Jung, O.-S.; Park, S. H.; Kim, K. M.; Jang, H. G. *Inorg. Chem*. **1998**, *37*, 5781−5785.
(18) Jung, O.-S.; Park, S. H.; Park, C. H.; Park, J. K. *Chem. Lett*. **1999**, 923−924.
(19) Constable, E. C. *Tetrahedron* **1992**, *48*, 10013−10059.
(20) Dunne, S. J.; Summers, L. A.; von Nagy-Felsobuki, E. I. *J. Mol. Struct. (Thermochim)* **1991**, *230*, 219−234.
(21) Dunne, S. J.; Summers, L. A.; von Nagy-Felsobuki, E. I. *J. Heterocycl. Chem.* **1992**, *29*, 851−858.
(22) Carlucci, L. C.; Ciani, G.; Gudenberg, D. W. V.; Proserpio, D. M. *Inorg. Chem*. **1997**, *36*, 3812−3813.
(23) Schmidtchen, F. P.; Berger, M. *Chem. Rev*. **1997**, *97*, 1609−1646.
(24) Beer, P. D. *Acc. Chem. Res*. **1998**, *31*, 71−80.

10.1021/ja001618b CCC: $19.00
Published on Web 09/28/2000

Table 1. Crystallographic Data for $[Ag(Py_2O)]NO_3$, $[Ag(Py_2O)]BF_4$, $[Ag(Py_2O)]ClO_4$, and $[Ag(Py_2O)]PF_6$[a]

	$[Ag(Py_2O)]NO_3$	$[Ag(Py_2O)]BF_4$	$[Ag(Py_2O)]ClO_4$	$[Ag(Py_2O)]PF_6$
formula	$C_{10}H_8N_3O_4Ag$	$C_{10}H_8N_2OBF_4Ag$	$C_{10}H_8N_2O_5ClAg$	$C_{10}H_8N_2OF_6PAg$
f*w*	342.06	366.86	379.50	425.02
space group	$P2_1/c$	$P2_1/c$	$P2_1/c$	$P2_1/n$
a, Å	11.021(1)	10.483(4)	10.553(1)	10.575(3)
b, Å	7.430(2)	8.933(1)	9.034(2)	9.621(2)
c, Å	13.721(2)	13.707(2)	13.708(2)	14.175(3)
β, deg	99.04(1)	104.72(2)	106.70(1)	109.80(1)
V, Å^3	1109.6(4)	1241.5(5)	1251.7(4)	1356.9(6)
Z	4	4	4	4
d_{cal}, gcm^{-3}	2.048	1.963	2.014	2.080
μ, mm^{-1}	1.827	1.664	1.841	1.672
$R\ \{I > 2\sigma(I)\}$	R1 = 0.0306	0.0547	0.0372	0.0352
	wR2 = 0.0829	0.1470	0.0968	0.0907

[a] $R1 = \sum||F_o| - |F_c||/\sum|F_o|$. $wR2 = \sum w(F_o^2 - F_c^2)^2/\sum wF_o^4)^{1/2}$.

Junsei Chemical Co., respectively, and used as received. 3,3′-Oxybispyridine (Py_2O) was prepared by the literature procedure.[25] Elemental microanalyses (C, H, N) were performed on crystalline samples by the Advanced Analytical Center at KIST using a Perkin-Elmer 2400 CHNS analyzer. X-ray powder diffraction data were recorded on a Rigaku RINT/DMAX-2500 diffractometer at 40 kV and 126 mA for Cu Kα. Thermal analyses were performed under N_2 at a scan rate of 5 °C/min using a Stanton Red Croft TG 100. Infrared spectra were obtained on a Perkin-Elmer 16F PC FTIR spectrophotometer with samples prepared as KBr pellet. Ion concentrations were measured on a Dionex 300 ion chromatograph (flow rate = 1.2 mL/min).

Direct Preparation of $[Ag(Py_2O)]X$ ($X^- = BF_4^-$, NO_3^-, ClO_4^-, and PF_6^-). $[Ag(Py_2O)]BF_4$: A methanol solution (6 mL) of Py_2O (52 mg, 0.3 mmol) was slowly diffused into an aqueous solution (6 mL) of $AgBF_4$ (58 mg, 0.3 mmol). Colorless crystals of $[Ag(Py_2O)]BF_4$ formed at the interface, and were obtained in 3 days in 80% yield. Anal. Calcd for $C_{10}H_8N_2OBF_4Ag$: C, 32.74; H, 2.20; N, 7.64. Found: C, 32.70; H, 2.18; N, 7.64. IR (KBr, cm^{-1}): $\nu(BF_4)$ 1088 (s, multibands). Using acetone or ethanol instead of the methanol, the same crystals were obtained. The similar treatment of AgX ($X^- = NO_3^-$, ClO_4^-, and PF_6^-) with Py_2O afforded $[Ag(Py_2O)]NO_3$, $[Ag(Py_2O)]ClO_4$, and $[Ag(Py_2O)]PF_6$, respectively. **$[Ag(Py_2O)]NO_3$:** Yield, 75%. Anal. Calcd for $C_{10}H_8N_3O_4Ag$: C, 35.11; H, 2.36; N, 12.28. Found: C, 35.0; H, 2.33; N, 12.40. IR (KBr, cm^{-1}): $\nu(NO_3)$ 1384(s). **$[Ag(Py_2O)]ClO_4$:** Yield, 81%. Anal. Calcd for $C_{10}H_8N_2O_5ClAg$: C, 31.65; H, 2.12; N, 7.34. Found: C, 31.80; H, 2.12; N, 7.38. IR (KBr, cm^{-1}): $\nu(ClO_4)$ 1088 (s, multibands). **$[Ag(Py_2O)]PF_6$:** Yield, 84%. Anal. Calcd for $C_{10}H_8N_2OPF_6Ag$: C, 28.26; H, 1.90; N, 6.59. Found: C, 28.20; H, 1.88; N, 6.46. IR (KBr, cm^{-1}): $\nu(PF_6)$ 836(s, br).

Counteranion Exchange. The procedure of a typical counteranion exchange is outlined: An aqueous solution (5 mL) of $NaBF_4$ (35 mg, 0.32 mmol) was added to a suspension of microcrystalline $[Ag(Py_2O)]NO_3$ (36 mg, 0.10 mmol) in water (5 mL) at room temperature. The reaction mixture was stirred, and the precipitates after 1, 3, 6, 12, and 24 h were monitored by IR spectra. After 24 h, the reaction mixture was filtered and washed with several aliquots of water and methanol. Found for $[Ag(Py_2O)]BF_4$ prepared by the counteranion exchange: C, 32.60; H, 2.21; N, 7.54. The counteranion exchange of $[Ag(Py_2O)]NO_3$ with ClO_4^- as well as PF_6^- was similarly achieved. Found for $[Ag(Py_2O)]ClO_4$ prepared by the exchange: C, 31.40; H, 2.09; N, 7.24. Found for $[Ag(Py_2O)]PF_6$ prepared by the exchange: C, 28.10; H, 1.90; N, 6.39. Found for $[Ag(Py_2O)]NO_3$ prepared by the counteranion exchange of $[Ag(Py_2O)]BF_4$ with NO_3^-: C, 34.70; H, 2.28; N, 12.40. The exchanged species still give a sharp X-ray powder diffraction pattern. The IR spectra, X-ray powder diffraction patterns, and elemental analyses of the exchanged species are compared with those of the corresponding compounds prepared from the direct reaction.

Crystallographic Structure Determinations. $[Ag(Py_2O)]NO_3$ was prepared by the counteranion exchange of $[Ag(Py_2O)]BF_4$ with NO_3^- ions, and the exchanged species was recrystallized in water to obtain X-ray quality colorless crystals (0.35 × 0.20 × 0.07 mm). The colorless crystals of $[Ag(Py_2O)]BF_4$ were obtained by the treatment of $AgBF_4$ with Py_2O (0.30 × 0.28 × 0.20 mm). The colorless crystals of $[Ag(Py_2O)]ClO_4$ were obtained by the reaction of $AgClO_4$ with Py_2O (0.20 × 0.20 × 0.20 mm). The colorless crystals of $[Ag(Py_2O)]PF_6$ were obtained by the reaction of $AgPF_6$ with Py_2O (0.38 × 0.35 × 0.20 mm). All X-ray data were collected on an Enraf-Nonius CAD4 automatic diffractometer with graphite-monochromated Mo Kα (λ = 0.71073 Å) at ambient temperature. Unit cell dimensions were based on 25 well-centered reflections by using a least-squares procedure. All crystals form in the monoclinic crystal system. During the data collection, three standard reflections monitored after every hour did not reveal any systematic variation in intensity. The structures were solved by the SHELXS 97,[26] followed by successive difference Fourier synthesis. The non-hydrogen atoms were refined anisotropically and hydrogen atoms were placed in calculated positions and refined only for the isotropic thermal factors. All calculations were carried out on a personal computer with use of SHELXS 97 and SHELXL 97. Crystal parameters and procedural information corresponding to data collection and structure refinement were given in Table 1. Atomic positions and equivalent isotropic thermal parameters are available in Supporting Information.

Results

Construction and Crystal Structures of Helices. Our strategy for constructing and operating the molecular spring was schematically depicted in Figure 1. The skewed (θ) conformational Py_2O ligand is a key tectonic element for self-assembly of the cylindrical helices by coordination to the liner directional silver(I) ion. On the basis of this design strategy, the slow diffusion of a methanolic solution of Py_2O into an aqueous solution of AgX ($X^- = BF_4^-$, NO_3^-, ClO_4^-, and PF_6^-) in a 1:1 stoichiometry afforded single crystals of the composition of $[Ag(Py_2O)]X$ in high yields. The construction of the skeletal structure was not significantly affected by the change of the mole ratio, solvents, and concentration.

X-ray crystallographic characterization reveals infinite cylindrical helices shown in Figure 2. Selected bond lengths and angles are listed in Table 2. The helix consists of a single strand of alternating Ag(I) and Py_2O, and there are two of these units in each turn (2_1 along the *b* axis). The oblong cylindrical helices (the shortest intrahelical Ag···Ag, 6.42−7.23 Å × the shortest intrahelical O···O, 9.26−9.53 Å) are arrayed in alternate right-handed and left-handed fashion (Figure 2b), which is similar to the results of Ciani et al.[27] Interestingly, the counteranions are pinched in two columns between/inside the helical pitch,

(25) Barker, D. J.; Summers, L. A. *J. Heterocycl. Chem.* **1983**, *20*, 1411−1412.

(26) Sheldrick, G. M. SHELXS-97: A Program for Structure Determination; University of Götingen, Germany, 1997. Sheldrick, G. M. SHELXL-97: A Program for Structure Refinement; University of Götingen, Germany, 1997.

(27) Carlucci, L.; Ciani, G.; Proserpio, D. M.; Sironi, A. *Inorg. Chem.* **1998**, *37*, 5941−5943.

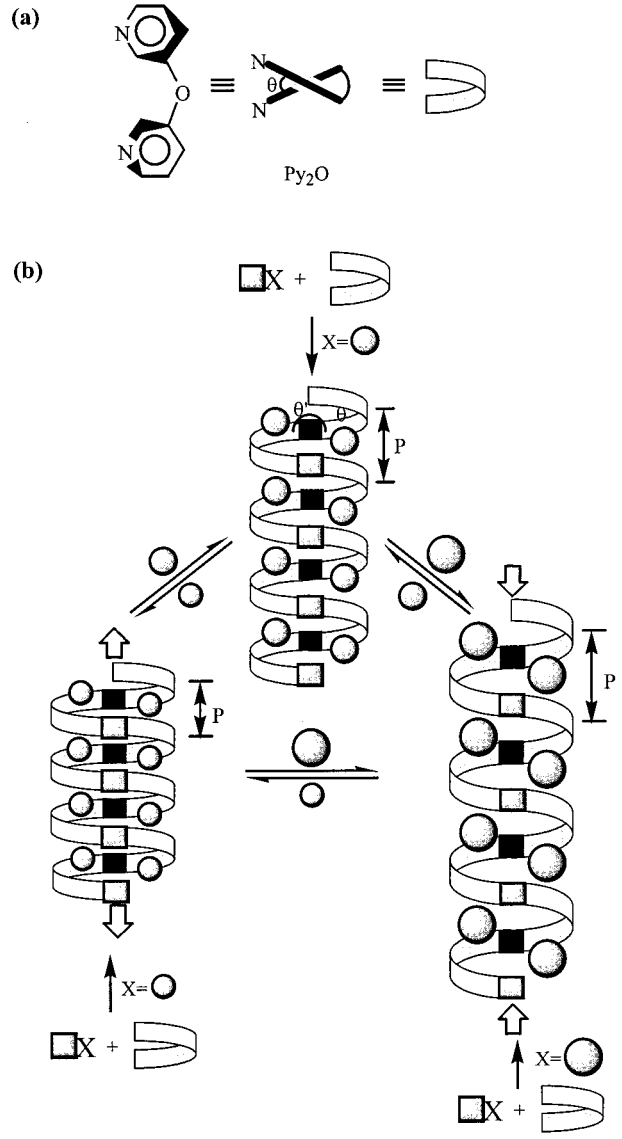

Figure 1. (a) Schematic diagram of the stable skewed conformational Py_2O. (b) Design for the molecular spring from a combination of the linear geometric silver(I) ion and the skewed Py_2O spacer. The tunable pitch via the counteranion exchange.

probably due to the presence of the weak electrostatic interactions between the Ag(I) cations and their counteranions (the shortest Ag···F, Ag···O, 2.66−2.86 Å). The counteranion exchange of $[Ag(Py_2O)]BF_4$ with the smaller planar NO_3^- afforded $[Ag(Py_2O)]NO_3$. The exchanged species was recrystallized in water to obtain the crystals suitable for X-ray crystallography. The structure of the exchanged $[Ag(Py_2O)]NO_3$ is basically similar to that of $[Ag(Py_2O)]BF_4$, but the helical pitch of $[Ag(Py_2O)]NO_3$ (7.430(2) Å) shortens relative to that of $[Ag(Py_2O)]BF_4$ (8.933(1) Å: the crystallographic *b* axis). The crystal structures of $[Ag(Py_2O)]ClO_4$ and $[Ag(Py_2O)]PF_6$ are also the same cylindrical helices. Thus, the skeletal structures of all complexes with the NO_3^-, BF_4^-, ClO_4^-, and PF_6^- series are similar helices. A salient feature is that each helical pitch is proportional to the volume of the counteranion guest. In particular, the crystal structure of the exchanged $[Ag(Py_2O)]NO_3$ shows that the helical structure is still retained after the counteranion exchange. Another feature is the interspring Ag···Ag distances (3.345(1)−3.638(1) Å) which are similar to the van der Waals radii (3.44 Å) and the known ligand-unsupported

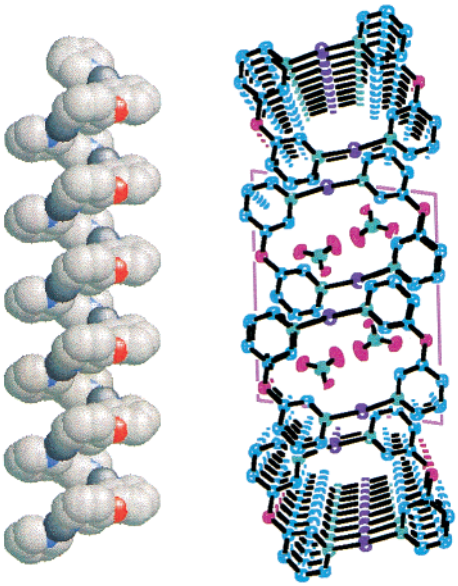

Figure 2. Crystal structure of $[Ag(Py_2O)]NO_3$. (a) Space-filling representation of the helical spring. Deep gray, red, blue, and gray correspond to Ag, O, N, and C atoms, respectively. The counteranions were omitted for clarity. (b) Packing top view of the molecular springs, emphasizing the cylindrical helix and the nitrate anions inside the springs in the unit cell. Purple, red, green, and blue correspond to Ag, O, N, and C atoms, respectively.

Table 2. Selected Bond Lengths (Å) and Angles (deg) for $[Ag(Py_2O)]NO_3$, $[Ag(Py_2O)]BF_4$, $[Ag(Py_2O)]ClO_4$, and $[Ag(Py_2O)]PF_6$

	$[Ag(Py_2O)]$-NO_3	$[Ag(Py_2O)]$-BF_4	$[Ag(Py_2O)]$-ClO_4	$[Ag(Py_2O)]$-PF_6
Ag−N(1)	2.139(4)	2.145(4)	2.150(4)	2.125(3)
Ag−N(2)	2.138(4)	2.137(4)	2.148(4)	2.136(3)
Ag···Ag′	3.345(1)	3.347(1)	3.360(1)	3.638(1)
N(1)−Ag−N(2)	173.1(1)	172.5(2)	172.8(1)	172.6(1)
C−O−C	121.3(3)	119.7(4)	118.1(3)	120.2(3)

closed-shell d^{10} Ag···Ag interactions.[28] The slightly bent angles of N−Ag−N (172.5(2)−173.1(1)°) support the presence of the weak metal−metal interactions. Thus, the local geometry around the silver ion may be best described as "a leaning *T*".

Tuning of Helical Pitch via Anion Exchange. Although the helix suggests an ideal spring structure, it does not by itself prove that the helix behaves as a molecular spring. For the cationic cylindrical helix, the counteranion exchange should be able to reversibly tune the helical pitch by control of the total dihedral angle ($\theta + \theta'$) (Figure 1b). Initial evaluation revealed that the counteranion exchange of $[Ag(Py_2O)]BF_4$ with NO_3^- smoothly occurs. The reverse exchange was easily achieved under the same conditions. The anions of NO_3^- (36.0 cm^3/mol), BF_4^- (51.0 cm^3/mol), ClO_4^- (52.1 cm^3/mol), and PF_6^- (56.2 cm^3/mol) exhibit substantial differences in size (Table 3). Nevertheless, the BF_4^- counteranions within the helix were completely exchanged with the bulkier octahedral PF_6^- anions as well as the similar tetrahedral ClO_4^- anions. To investigate the exchange procedure, the counteranion exchange of $[Ag(Py_2O)]NO_3$ with ClO_4^- was monitored by the characteristic IR bands of counteranions.[29] The counteranion exchange in water at room temperature was checked after 4, 8, and 16 h (Figure 4a). The infrared spectrum shows the gradual disappearance of intense NO_3^- peaks (1400−1320 cm^{-1}) and the

(28) Singh, K. S.; Long, J. R.; Stavropoulos, P. *J. Am. Chem. Soc.* **1997**, *119*, 2942−2943.
(29) Yaghi, O. M.; Li, H. *J. Am. Chem. Soc.* **1996**, *118*, 295−296.

Table 3. Structural and Physicochemical Data

compounds	guest anion vol[a] (cm^3/mol)	dihedral angle[b] (deg)	helical pitch (Å)	Ag···Ag distance (Å)[c]	ρ_{cal}[d]
$[Ag(Py_2O)]NO_3$	36.0	56.6(1) + 8.6(2) = 65.2(3)	7.430(2)	3.345(1)	2.048
$[Ag(Py_2O)]BF_4$	51.0	74.3(2) + 14.5(4) = 88.8(6)	8.933(1)	3.347(1)	1.963
$[Ag(Py_2O)]ClO_4$	52.1	77.2(2) + 12.9(3) = 90.1(5)	9.034(2)	3.360(1)	2.014
$[Ag(Py_2O)]PF_6$	56.2	76.7(1) + 21.5(2) = 98.2(3)	9.621(2)	3.638(1)	2.080

[a] Calculated from the Gaussian 94 program (J. A. Pople et al.). [b] The dihedral angle between two pyridyl groups around O (θ) + the dihedral angle between two pyridyl groups around Ag (θ'). [c] Interspring silver(I)···silver(I) interaction. [d] Calculated density.

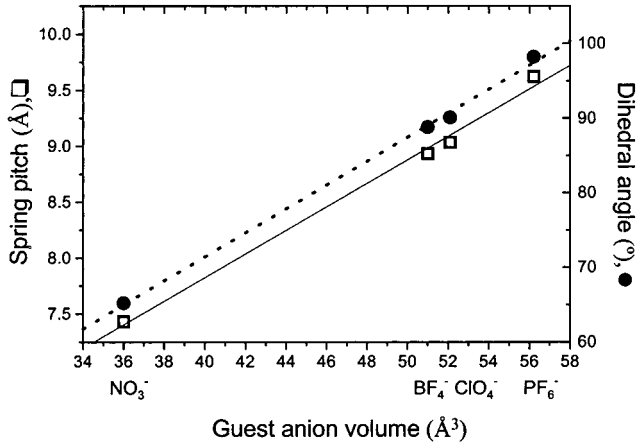

Figure 3. Plot of the spring-pitch (□) and the dihedral angle (●) as a function of the guest (X) volume in $[Ag(Py_2O)]X$ ($X^- = NO_3^-$, BF_4^-, ClO_4^-, and PF_6^-).

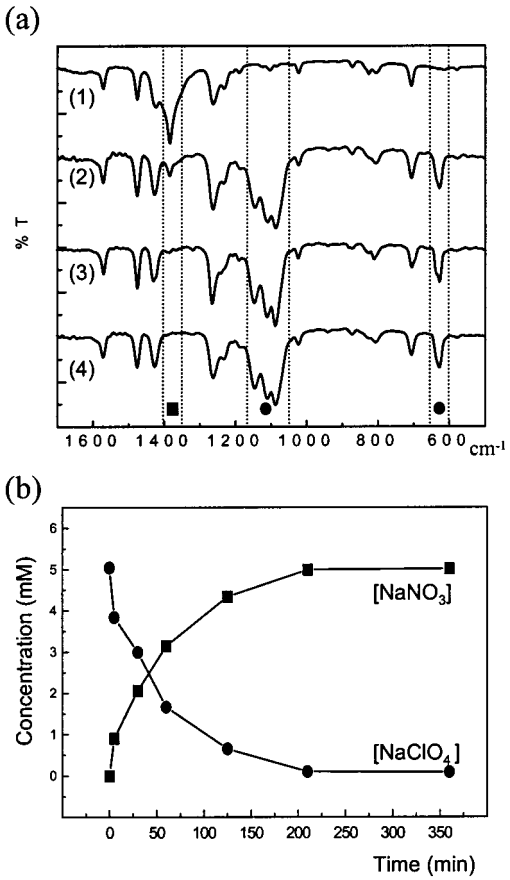

Figure 4. (a) IR (KBr pellet) change procedure during the counteranion exchange of $[Ag(Py_2O)]NO_3$ with $NaClO_4$: (1) $[Ag(Py_2O)]NO_3$, (2) after 4 h, (3) after 8 h, and (4) after 16 h. (b) The $NaNO_3$ vs $NaClO_4$ concentration change during the counteranion exchange of $[Ag(Py_2O)]$-NO_3 (172 mg, 0.50 mmol) with $NaClO_4$ (5 mM; 31 mg/50 mL, 0.25 mmol). Each concentration after 0, 10, 30, 60, 120, 210, and 370 min was measured on a Dionex 300 ion chromatograph (flow rate = 1.2 mL/min)

appearance and growth of new ClO_4^- peaks (1170−1050 cm^{-1}). The NO_3^- peaks disappear completely after 16 h. The other peaks of the spectrum remain virtually unchanged. To monitor quantitatively the exchange efficiency vs the time, an excess of microcrystalline $[Ag(Py_2O)]NO_3$ was immersed in an aqueous solution (5 mL) of $NaClO_4$ (5 mM), and the mixture solution was stirred at room temperature. Each concentration of free anions ($NaNO_3$ and $NaClO_4$) in the solution was analyzed after 10, 30, 60, 120, 210, and 370 min. As the counteranion exchange proceeds, the concentration of free NO_3^- ions increases exponentially with the concomitant exponential decrease of free ClO_4^- ions (Figure 4b). The counteranions are easily exchanged, but the exchange rate is some or less dependent upon the counteranions, the reaction temperature, the mole ratio, and the concentration. For an instance, the exchange of $[Ag(Py_2O)]ClO_4$ with BF_4^- occurs very slowly at room temperature. The rate of counteranion exchange is dependent upon the solubility of the exchanged species when the mixtures of counteranions were used. The symmetrical nature of anions is a significant factor in retaining the skeletal helical structure. For our helical structure, the upper limit size is PF_6^-. All the exchanged species were characterized by the X-ray powder diffraction, elemental analysis, and IR spectrum. The X-ray powder diffraction patterns of $[Ag(Py_2O)]ClO_4$ prepared by the direct reaction and by the counteranion exchange of $[Ag(Py_2O)]NO_2$ and $NaClO_4$ are depicted in Figure 5. They show similar relative peak intensity and position, indicating clearly the retention of the skeletal structure after the counteranion exchange. Their data are consistent with those of the crystals obtained by the direct reaction of AgX ($X^- = NO_3^-$, BF_4^-, ClO_4^-, and PF_6^-) with Py_2O (Supporting Information).

Discussion

Why is our infinite molecular spring so effectively constructed and dynamically operated? Cooperative effects of the skewed conformer of the Py_2O and the linear N−Ag(I)−N bonds may contribute to a driving force for the formation of the ideal cylindrical helix. Such effects preferably adopt the helix irrespective of the present symmetric counteranions, the mole ratio, and concentration. However, the diffusion of $AgNO_3$ with Py_2O at high temperatures (>80 °C) gave a simple network structure. This appears to be primarily associated with a θ change in the Py_2O at the high temperatures, indicating that the reaction temperature is a significant factor in the construction of the helix. Especially, the X-ray crystal structures in combination with the counteranion exchange show that the helix is reversibly tuned without destruction of the skeleton within the flexible pitch-range (7.430(2)−9.621(2) Å). The lability of the counteranions allows their replacement by other anions, and the bulkiness of the replaced counteranion controls the dihedral angle between two pyridyl groups around the C−O−C (θ) and N−Ag−N (θ') bonds without any particular strain. The helical

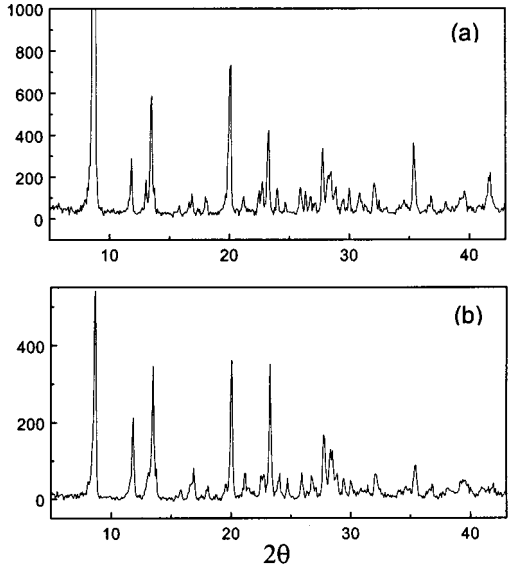

Figure 5. The X-ray powder diffraction patterns of $[Ag(Py_2O)]ClO_4$ prepared by the direct reaction a and by the counteranion exchange of $[Ag(Py_2O)]NO_2$ and $NaClO_4$ (b).

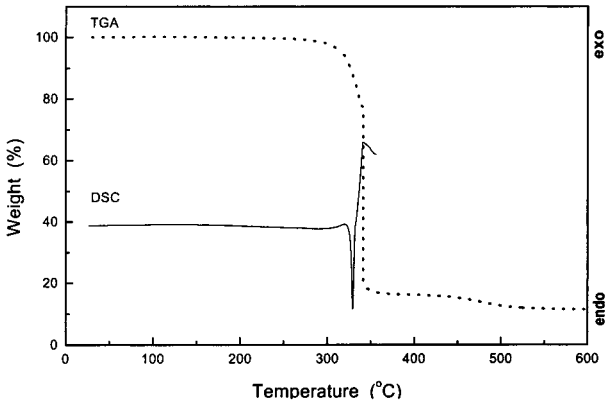

Figure 6. Overlay of TGA and DSC traces of $[Ag(Py_2O)]ClO_4$, each recorded at a heating rate of 5 °C min^{-1}.

pitch varies in length of about 0.11 Å per the unit volume (cm^3/mol) of the counteranion. Though all experiments including the preparation and the counteranion exchange are carried out either in aqueous solutions or in water-containing solutions, the infinite cationic helix contains no solvate water molecules. This fact implies a significant structural behavior, i.e., since the spring is agilely contracted or stretched by its counteranion exchange, there are no extra spaces that are large enough to accommodate other small guest molecules into the spring. This is clear from the calculated densities of the four crystals, which remain nearly invariant at the high values of ρ_{calcd} (1.963−2.080 g cm^{-3}) shown in Table 3. The high densities demonstrate that the molecular spring effectively bites all the counteranions. If the helix is not tunable, the counteranion exchange with the smaller anion gives extra spaces inside the helix. Moreover, the counteranion exchange with the bigger anions would not occur under the same conditions. The helical pitch, therefore, is directly dependent upon only the size of the counteranion.

The traces of thermogravimetric analysis (TGA) and differential scanning calorimetry (DSC) indicate that all the compounds have a reasonable degree of thermal stability (up to 231−332 °C) in the solid state. The TGA and DSC of all the compounds exhibit a similar pattern, but the thermal stability is affected by the kind of counteranion inside the helix (NO_3^-, 231 °C; BF_4^-, 322 °C; ClO_4^-, 330 °C; PF_6^-, 332 °C). Typical thermograms of $[Ag(Py_2O)]ClO_4$ are shown in Figure 6. $[Ag(Py_2O)]ClO_4$ melts at 330 °C and then decomposes exothermically just above that temperature. The endothermic peak at 330 °C is attributed to the melting point. All the compounds display sharp melting points, but immediately decompose just above the melting points. This fact indicates that the helical structure is unstable in the melting state, presumably due to the strain energy of the helix in that state. Thus, the decomposition temperatures of the helical series are directly related to their melting points. The melting points were also identified on a melting point apparatus. The helical compounds are stable for several days in pH 3.5−10.0 aqueous solution. According to the ^1H NMR spectrum of the slightly water-soluble $[Ag(Py_2O)]NO_3$ (Supporting Information), the bonds of Ag(I)−N still exist, but the retention of the helical structure is not clear in aqueous solution. Its temperature-dependent behavior in solution is observed. The other BF_4^-, ClO_4^-, and PF_6^- analogues are nearly insoluble in water and common organic solvents.

Conclusions

The present work is the first example to demonstrate that the pitch of the self-assembled helical spring can be tuned through the reversible incorporation of guest anions that differ in size. Our strategy for constructing and operating the molecular spring, to our knowledge, is an important conceptual advance. The helices are smart anion exchange materials that are extremely sensitive to the volume of anions. The tunable molecular spring will be intended to contribute to the development of molecular-based recognition materials such as sensor, molecular switch,[15,30] chemical separator, drug and chemical delivery, and DNA control.

Acknowledgment. This work was supported in part by the Ministry of Science and Technology in Korea (KIST2010).

Supporting Information Available: Crystallographic, IR, X-ray powder diffraction, TGA, and DSC data for $[Ag(Py_2O)]NO_3$, $[Ag(Py_2O)]BF_4$, $[Ag(Py_2O)]ClO_4$, and $[Ag(Py_2O)]PF_6$; temperature-dependent NMR spectra of $[Ag(Py_2O)]NO_3$ (PDF). This material is available free of charge via the Internet at http://pubs.acs.org.

JA001618B

(30) Gourdon, A. *New J. Chem.* **1992**, *16*, 953−957.